Bioactive Materials 19 (2023) 167–178

Contents lists available at ScienceDirect

Bioactive Materials

journal homepage: www.keaipublishing.com/en/journals/bioactive-materials

A bioactive compliant vascular graft modulates macrophage polarization and maintains patency with robust vascular remodeling

Alexander Stahl [a,b,1], Dake Hao [c,d,1], Janos Barrera [e], Dominic Henn [e], Sien Lin [a], Seyedsina Moeinzadeh [a], Sungwoo Kim [a], William Maloney [a], Geoffrey Gurtner [e], Aijun Wang [c,d,f,*], Yunzhi Peter Yang [a,g,h,**]

[a] Department of Orthopaedic Surgery, Stanford University, 240 Pasteur Drive, Stanford, CA, 94304, USA
[b] Department of Chemistry, Stanford University, 121 Mudd Building, Stanford, CA, 94305, USA
[c] Department of Surgery, School of Medicine, University of California Davis, Sacramento, CA, 95817, USA
[d] Institute for Pediatric Regenerative Medicine, Shriners Hospitals for Children, Sacramento, CA, 95817, USA
[e] Department of Surgery, Stanford University, 300 Pasteur Drive, Stanford, CA, 94305, USA
[f] Department of Biomedical Engineering, University of California Davis, Davis, CA, 95616, USA
[g] Department of Materials Science and Engineering, Stanford University, 496 Lomita Mall, Stanford, CA, 94305, USA
[h] Department of Bioengineering, Stanford University, 443 Via Ortega, Stanford, CA, 4305, USA

ARTICLE INFO

Keywords:
Vascular graft
Vascular compliance
Pore size
Macrophage polarization
Vascular remodeling

ABSTRACT

Conventional synthetic vascular grafts are associated with significant failure rates due to their mismatched mechanical properties with the native vessel and poor regenerative potential. Though different tissue engineering approaches have been used to improve the biocompatibility of synthetic vascular grafts, it is still crucial to develop a new generation of synthetic grafts that can match the dynamics of native vessel and direct the host response to achieve robust vascular regeneration. The size of pores within implanted biomaterials has shown significant effects on macrophage polarization, which has been further confirmed as necessary for efficient vascular formation and remodeling. Here, we developed biodegradable, autoclavable synthetic vascular grafts from a new polyurethane elastomer and tailored the grafts' interconnected pore sizes to promote macrophage populations with a pro-regenerative phenotype and improve vascular regeneration and patency rate. The synthetic vascular grafts showed similar mechanical properties to native blood vessels, encouraged macrophage populations with varying M2 to M1 phenotypic expression, and maintained patency and vascular regeneration in a one-month rat carotid interposition model and in a four-month rat aortic interposition model. This innovative bioactive synthetic vascular graft holds promise to treat clinical vascular diseases.

1. Introduction

Clinically, synthetic vascular grafts under 6 mm in diameter experience high long-term failure rates, in large part due to thrombosis and intimal hyperplasia associated with disturbed hemodynamics and compliance mismatch between the native vessel and stiffer graft materials [1–4]. In humans, these non-degradable synthetic grafts often fail to significantly regenerate vascular tissues on the luminal surface and within the graft walls, even after prolonged implantation periods [5]. A functional synthetic vascular graft with mechanical properties capable of better matching the dynamics of the native blood vessel wall with enhanced vascular regenerative potential could expand treatment options for common cardiovascular diseases and could even find future applications as part of vascularized engineered tissues and organs.

Despite a great deal of research towards developing improved synthetic small diameter vascular grafts (SDVG), only a handful have

Peer review under responsibility of KeAi Communications Co., Ltd.
* Corresponding author. Department of Surgery, School of Medicine University of California Davis, Research II, Suite 3005, 4625 2nd Avenue, Sacramento, CA, 95817, United States.
** Corresponding author. Department of Orthopedic Surgery, School of Medicine, Stanford University, 240 Pasteur Drive, BMI 258, Stanford, CA, 94304, USA.
E-mail addresses: aawang@ucdavis.edu (A. Wang), ypyang@stanford.edu (Y.P. Yang).
[1] equal contribution by authors.

https://doi.org/10.1016/j.bioactmat.2022.04.004
Received 30 November 2021; Received in revised form 14 March 2022; Accepted 5 April 2022

progressed past initial *in vivo* trials. Many studies of SDVG monitor implantation for 1 month or less, and the median implantation duration in large animal studies is only 56 days [6]; the majority of engineered grafts therefore either do not move on to later stage trials or else the results of any follow-up studies are not reported. These statistics are not surprising, given the low success rates of the synthetic SDVG reported in the literature, with more than 75% occluding [6]. Tissue engineering strategies such as fabricating grafts from bioresorbable materials that can gradually be replaced by native tissues show promise to overcome some of the current limitations of clinical synthetic grafts. And materials designed to better match the mechanics of the vessel wall could reduce the risks of pathological graft responses while the material remains.

In addition to the mechanical dynamics, material features such as the structure and morphology of the scaffolds have received increasing attention for tissue regeneration [7–10]. Pore sizes within the implanted material have been accepted as an important factor influencing macrophage polarization, which further regulate tissue regeneration including vascular remodeling [11]. Allowedly, M1 phenotype macrophages stimulate host immune reactions, while the M2 phenotype macrophages resolve inflammation and participate in the tissue remodeling process. Hence, designing vascular grafts capable of promoting higher levels of M2 macrophages compared with M1 macrophages is a promising strategy to promote the remodeling of vascular grafts. Previous studies investigating the effects of biomaterials with different pore sizes on macrophage polarization have found, for instance, that increasing the pore size from 1.92 to 29.46 μm stimulated macrophage polarization toward an M2 phenotype [12]. Similarly, Sussman et al. found that macrophages on implanted biomaterials with interconnected pore structures showed higher expression of M2 markers when the average pore size was 160 μm compared with implants having a pore size of 34 μm. Interestingly, the authors found that direct contact between macrophages and the biomaterial surface may promote the M1 phenotype, which can account for the greater number of M1 macrophages in scaffolds with a smaller pore size and higher surface area [13]. These results indicate that biomaterial pore sizes ranging from tens to hundreds of microns is of research significance for macrophage polarization.

Beyond the specific effects on macrophage polarization, pore size in biomaterial scaffolds has also been found to impact the rate of cellular ingrowth and tissue regeneration. A minimum pore size of 25–40 μm has been suggested as a threshold for cellular invasion, below which only minimal ingrowth is observed [5,14,15]. Oliviero et al. propose that pore sizes of approximately 35–100 μm are optimal for blood vessel formation within a scaffold [16], though evidence from Boersema et al. suggests that the effect of pore size and structure on tissue regeneration may not necessarily be the same in scaffolds made from different materials [17].

We previously reported the development of a slowly bioresorbable polyurethane elastomer containing polycaprolactone (PCL) and the antiplatelet drug dipyridamole [18]. Inclusion of the polyfunctionalized small drug molecule introduced crosslinks in the polymer chains, by which a highly elastic and strong material with an elastic modulus in the range of native vessel walls was obtained; and the antiplatelet activity of the monomer reduced platelet adhesion on dipyridamole-containing polyurethane (DPY-PU) structures. The DPY-PU demonstrated cytocompatibility, supporting vascular cell proliferation, and hemocompatibility, through reduced platelet adhesion and activation.

In the current study, we fabricated porous synthetic DPY-PU vascular grafts with different pore sizes, 30–50 μm, 50–80 μm and 80–200 μm, to serve as synthetic vessel surrogates. The bioactive potential of our grafts to mediate the macrophage M1-to-M2 transition through pore size interactions was optimized in a one-month rat carotid artery interposition model. The mid-term patency and vascular remodeling of the optimized synthetic DPY-PU vascular grafts were then evaluated in a four-month rat aorta interposition model. We hypothesized that these vascular grafts, designed with tailored material properties and pore size, would promote vascular regeneration and maintain longer-term patency.

2. Results and discussion

2.1. Graft fabrication and characterization

SDVG were fabricated using a heat cure/porogen extraction molding technique to obtain an elastic polymer tube with an interconnected porous network extending across the graft wall. Pore size in TE scaffolds has been shown to impact the ingrowth and development of cells and tissues within TE constructs generally and in vascular grafts specifically. Below a pore size of 15 μm, sparse cellular penetration into porous SDVG has been observed [5,14,15]. Above this threshold, larger pore sizes correlate with faster invasion by capillaries and other tissues [5,19] and can influence cellular proliferation [20,21], and differentiation [21–23]. We constructed grafts with three different pore sizes using NaCl porogens of varying grain size: small (30–50 μm), medium (50–80 μm), and large (80–200 μm) to examine the optimal pore size range for tissue regeneration within the new DPY-PU grafts, while still maintaining desired graft mechanics and preventing blood leakage.

Scanning electron microscopy (SEM) and micro-computed tomography (micro-CT) confirmed removal of the porogen during the salt-leaching process, leaving behind interconnected pore networks (Fig. 1 A). The inner and outer surfaces of the grafts consist of thin polymer skins punctuated by randomly distributed pores, enabling cellular invasion from both the luminal blood and the surrounding solid tissues. The porogen size was found to be unrelated to the graft overall porosity, inner diameter, and wall thickness. Unlike uncrosslinked PCL, which has a relatively low melting point, the DPY-PU grafts are stable at high temperatures due to their thermoset nature and maintain their structural features during autoclave sterilization, an extremely useful feature in off-the-shelf medical devices.

Mechanical testing was performed to confirm the grafts were suitable for implantation and to evaluate whether different pore sizes affected the SDVG mechanics (Fig. 1 B). Stress-strain curves demonstrated that the grafts undergo elastic deformation well beyond the maximum extension experienced by native blood vessels (circumferential strains up to 17% have been reported in the rat abdominal aorta [24]), which is important for avoiding plastic deformation or breakage under physiological conditions. Stress-strain curves for native rat blood vessels have previously been reported [25]. As expected, uniaxial tensile testing demonstrated that the effective elastic moduli (E) of the porous graft structures (small pores $E = 0.27 \pm 0.08$ MPa, medium pores $E = 0.24 \pm 0.07$ MPa, large pores $E = 0.21 \pm 0.05$ MPa) were significantly reduced from the modulus of the non-porous material ($E = 1.26 \pm 0.07$ MPa), though the effective moduli of porous grafts has been known to increase postoperatively with the filling of pores [26]. To quantify SDVG compliance and burst pressure, grafts were attached to a water pressurization chamber and monitored under increased intraluminal pressure. Water leakage through the porous walls was prevented by plugging the graft pores with a layer of fibrin sealant to mimic the fibrin clot that forms within SDVG pores *in vivo*. Graft compliance (in % per 100 mmHg: 5.5 ± 2.9 for small pores, 8.5 ± 4.5 for medium pores, 10.1 ± 4.1 for large pores) was substantially greater than current synthetic medical SDVG and fell within the range of native vessel tissues, which is critical for maintaining undisturbed hemodynamics. Burst pressure measurements were underestimated due to the leaking of water through the weaker fibrin at elevated pressures, which in many cases prevented rupture of the DPY-PU membrane. Yet the grafts still demonstrated the capacity to withstand internal pressures great enough for use within the rat carotid artery and aorta. Uniaxial tensile testing measured rupture of the graft wall at stress levels of 0.47 ± 0.08 MPa for small pore grafts, 0.66 ± 0.33 MPa for medium pore grafts, and 0.26 ± 0.07 MPa for large pore grafts, which is comparable to the burst pressure of the native rat aorta (0.46 ± 0.07 MPa) [27]. Suture retention testing similarly confirmed the SDVG were tough enough to withstand surgical handling, with mean values of the porous DPY-PU ranging between 0.66 and 0.74 N, similar to the suture retention values of approximately 0.7 N reported

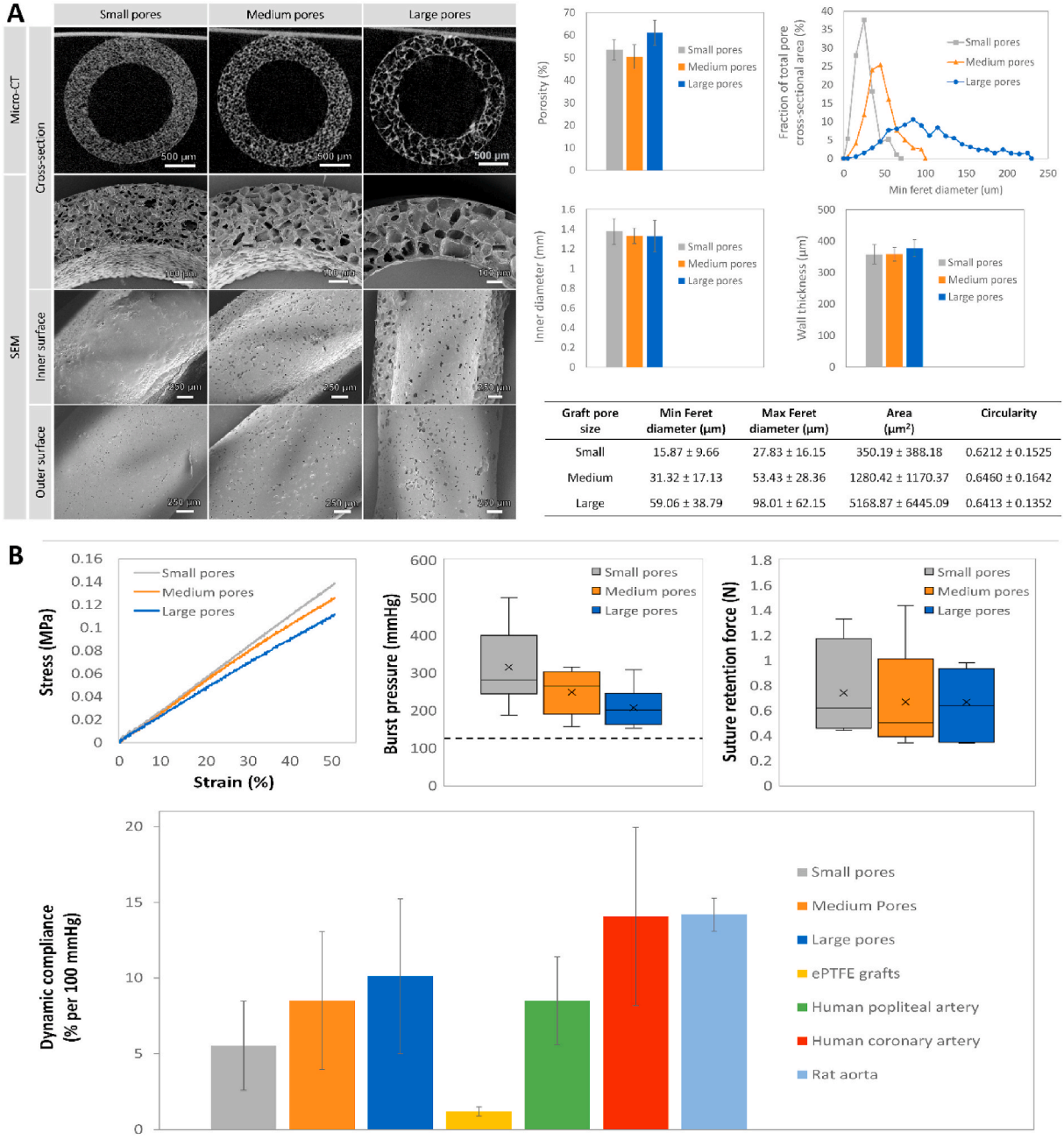

Graft pore size	Min Feret diameter (μm)	Max Feret diameter (μm)	Area (μm²)	Circularity
Small	15.87 ± 9.66	27.83 ± 16.15	350.19 ± 388.18	0.6212 ± 0.1525
Medium	31.32 ± 17.13	53.43 ± 28.36	1280.42 ± 1170.37	0.6460 ± 0.1642
Large	59.06 ± 38.79	98.01 ± 62.15	5168.87 ± 6445.09	0.6413 ± 0.1352

Fig. 1. Graft morphology and mechanical characterization. (A) Micro-CT and SEM analysis of the graft microstructure. Porosity (n = 10) was determined by micro-CT. Inner diameter (n = 7) and wall thickness (n = 7) were determined by SEM. Table shows mean (±S.D.) pore characteristics determined from SEM images. (B) Mechanical characterization of the porous DPY-PU SDVG: representative stress-strain curves, burst pressure (n = 10), suture retention (n = 7), and dynamic compliance of DPY-PU SDVG (n = 15) compared with medical Teflon (ePFTE) grafts [31], the human popliteal artery [32], human coronary artery [33], and rat aorta [34]. Although some trends were observed, no statistically significant difference was found between the DPY-PU grafts of different pore sizes. (x) In the box-and-whisker plots denotes the mean. Dashed line marks typical systolic blood pressure in normotensive rats [35]. Additional mechanical data can be found in supplementary information (Fig. S2).

for the jugular vein and 1.2 N for the rat carotid artery [28]. Unlike previous degradable synthetic SDVG made from elastomers tailored to match native vessel compliance [27,29], the DPY-PU grafts are robust enough to retain sutures and tolerate the pressures of the cardiovascular system without a dense external reinforcing layer, which constricts the distensibility of the inner elastic layer and often lacks sufficient porosity for cellular infiltration from the graft outer surface. Few materials are both strong and compliant enough to match native arteries [30], our DPY-PU grafts therefore demonstrate an uncommon combination of high elasticity, strength, and interconnected porosity between both surfaces, uniquely suited for small diameter vascular tissue engineered synthetic grafts.

We had previously demonstrated that non-porous DPY-PU material surfaces support cell adhesion and proliferation [18]. To confirm the ability of cells to populate the porous grafts, culture of human umbilical vein endothelial cells (HUVEC) and human mesenchymal stem cells (hMSC) was carried out on the porous membranes *in vitro* (supplementary information; Fig. S3). Both endothelial cells and MSCs proliferated on the DPY-PU scaffolds, with no statistically significant differences found based on pore size. Endothelial cells (EC) form the blood-contacting inner layer of native blood vessels and are involved in the regulation of vascular homeostasis, patency, and inflammation.

Thus, lack of a functional endothelial lining in vascular grafts is associated with decreased graft patency [36]. In large blood vessels, EC also form capillary networks within the vessel wall and are crucial to mural cell survival. The importance of EC in vascular health has led to multiple strategies to encourage EC growth in SDVG including pre-seeding graft lumens [37] or incorporating EC homing factors [38]. MSC, meanwhile, are multipotent stromal cells with many applications in regenerative medicine. MSC seeded on tissue engineered grafts can promote vascular healing through the release of growth factors and may also contribute to tissue regeneration through their own differentiation to vascular cells such as endothelial or smooth muscle cells [39]. The ability of DPY-PU grafts to support HUVEC and hMSC signal they are compatible with multiple promising strategies for regenerating healthy vascular tissues.

2.2. Implantation: patency and tissue regeneration

To investigate the ability of the SDVG to maintain blood flow and support tissue regeneration, grafts were implanted in a rat carotid interposition model and a rat abdominal aortic interposition model. Grafts with an inner diameter (ID) of 1.1–1.2 mm were selected for implantation in the rat left common carotid artery and larger diameter grafts (ID = 1.4–1.5 mm) were used in the rat aorta.

Short-term patency and tissue regeneration of SDVG were evaluated using a rat carotid interposition model. SDVG were implanted into the rat left common carotid artery and examined at 1 week and 4 weeks after implantation with 3 animals per group at 1 week and 6 animals per group at 4 weeks. After surgery, blood flow was observed immediately at both the proximal and distal ends of the grafts. All animals survived after the blood vessel replacement procedure. To investigate whether pore size exerts an effect on acute thrombosis within the grafts, no heparin was administered during surgery or postoperatively. SDVG handled well during surgery and no blood leakage was observed after implantation (at 0 week) (Fig. 2 A). The implantation of grafts for 1 week confirmed all grafts were patent (patency rate of small pores was 100%, 3/3; patency rate of medium pores was 100%, 3/3; patency rate of large pores was 100%, 3/3). The implantation of grafts for 4 weeks revealed grafts of all three groups retained high patency rate (more than 80%), and the patency rate of grafts in the medium pore (100%, 6/6) and large pore (100%, 6/6) groups were higher than in the small pore group (83%, 5/6) (Fig. 2 B).

H&E staining results revealed the presence of cells throughout the graft wall in all the three groups at 1 week and 4 weeks (Fig. 2C). At 1 week, a thin layer of neotissue had formed on the luminal surface of small pore grafts, but hardly any neotissue had formed on the luminal surface of both medium pore and large pore grafts. At 4 weeks, neotissue had formed on the luminal surface of all three graft groups (Fig. 2C). Quantification of lumen patency showed a significantly greater patent cross-sectional area was maintained in both medium pore and large pore grafts than in small pore grafts at 1 week and 4 weeks (Fig. 2 D). Quantification of the cell numbers in the graft wall, neointimal thickness, and the number of capillaries in grafts was performed. The results showed that more cells penetrated into the wall of the grafts as the pore size increased, and the grafts with medium and large pores significantly decreased the thickness of neointima and increased the number of capillaries in the grafts (Fig. S4). At 4 weeks, the varying degrees of neointima present in the luminal surfaces of the grafts with different pore sizes is likely caused by the different morphology of the graft surface due to the different pore sizes [9]. During H&E analysis, we observed some dark brown-stained tissue in the grafts with small and medium pore sizes that were not present in the grafts with large pore size. To further investigate this point, we performed the Von Kossa Staining for the specimens in all the groups, and the results showed varying degrees of calcific deposition occurred in the grafts with small and medium pores, but no calcific deposition occurred in the grafts with large pores (Fig. S5), which indicates the grafts with large pores avoid calcific deposition compared to the grafts with small and medium pores.

Trichrome, pentachrome, and immunohistochemical staining were performed to evaluate the tissue remodeling of grafts at 4 weeks. Trichrome and pentachrome staining showed regions of developing concentric layers and traces of elastic fibers and collagen, which are the main components of the vascular structure (Fig. 3 A and Fig. S6). Further CD31 and α-SMA staining showed positive staining for the endothelial cell marker CD31 on the luminal surface and the smooth muscle cell marker α-SMA within the wall of the developing neovessel tissue, which was consistent with the native rat carotid artery (Fig. 3 B). The migration of ECs and SMCs plays an important role in vascular remodeling [40,41].

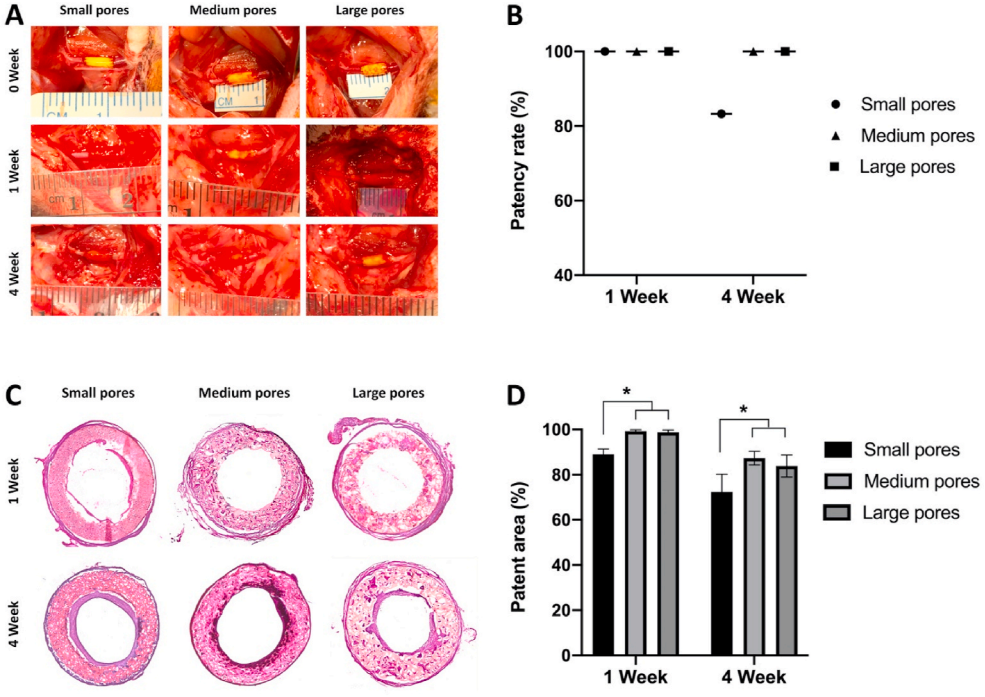

Fig. 2. Carotid interposition model. (A) DPY-PU SDVG implanted in rat left common carotid artery at various time points. (B) The patency rate of the grafts with different pore sizes at various time points. Each group at 1 week included 3 animals, and each group at 4 weeks included 6 animals. (C) H&E staining of the cross sections of the grafts with different pore sizes at various time points after implantation. (D) Quantification of the patent area of the grafts with different pore sizes at various time points after implantation. Each group at 1 week included 3 animals, and each group at 4 weeks included 6 animals. Data were expressed as mean ± standard deviation: *$p < 0.05$.

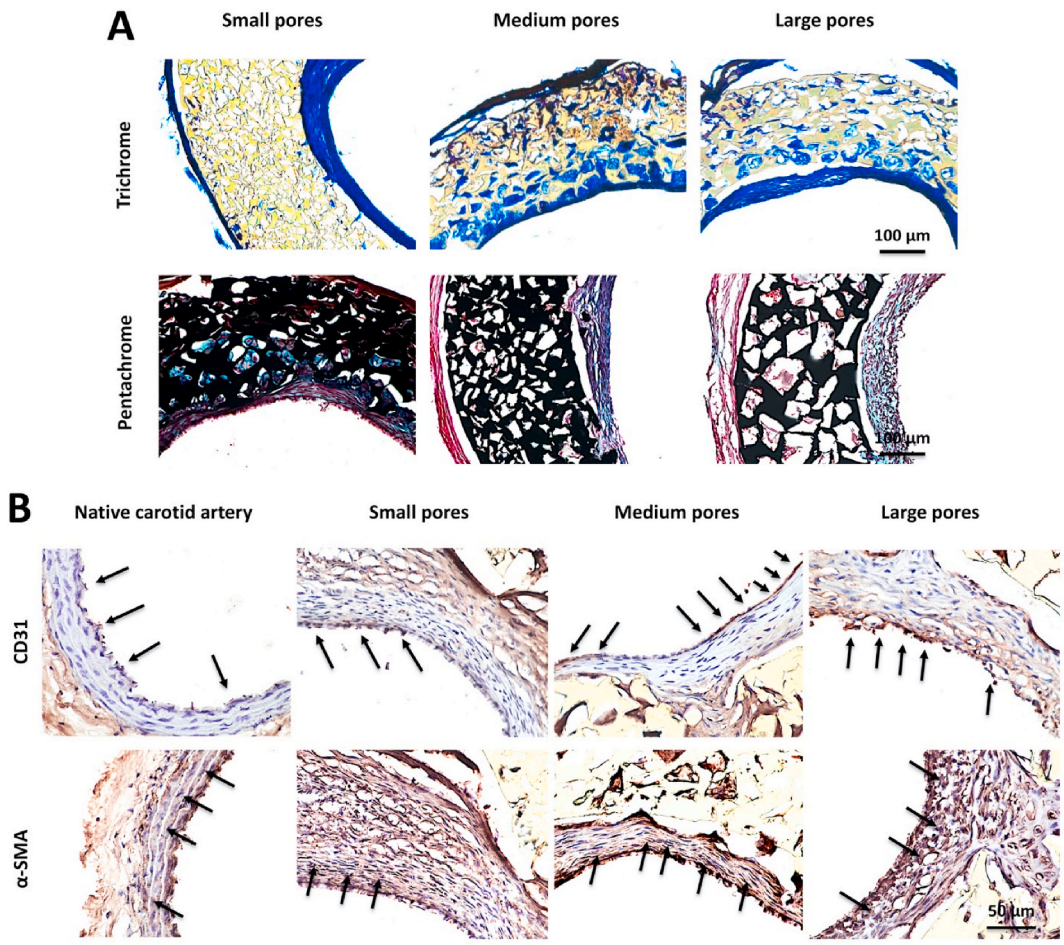

Fig. 3. (A) Trichrome and pentachrome staining of the grafts with different pore sizes at 4 weeks after implantation. Trichrome: cytoplasm and muscle fibers = red, collagen = blue, graft is yellow. Pentachrome: elastic fibers = black, nuclei = blue/black, collagen = yellow, mucin = bright blue, fibrin = bright red, muscle = red, graft stained black. (B) CD31 and α-SMA staining of the native rat carotid artery and the grafts with different pore sizes at 4 weeks after implantation. Yellow part indicated the graft. Arrows indicated the positive staining.

ECs and SMCs observed on the luminal surface of the grafts likely migrated from the surrounding native vascular tissue. Calponin and Smooth Muscle Myosin Heavy Chain (SM-MHC) staining were performed to characterize the SMC contractile phenotype. The results showed more SMCs with a contractile phenotype were present in the grafts with medium and larger pores compared to the grafts with small pores, and the largest number of contractile phenotype SMCs was present in the grafts with large pores (Fig. S7). These results indicated that our designed grafts with different pore sizes supported normal vascular regeneration.

Intense inflammatory response can inhibit vascular regeneration within implanted grafts, especially small diameter vascular grafts, in vascular replacement therapies. Regulation of the inflammatory response is a crucial challenge for long-term regeneration of vascularized grafts [42]. The process of tissue remodeling after implantation is always associated with a robust macrophage response that starts as early as a few days post-implantation. Polarized macrophages are referred to as either M1 or M2 cells, mimicking the Th1/Th2. M1 activated macrophages classically display proinflammatory activity, in contrast, M2 activated macrophages possess the ability to facilitate tissue repair and regeneration [43]. In addition, the pore size of scaffolds can be a critical regulator of macrophage phenotype, which further affects angiogenesis, vascularization, and other tissue regeneration processes. Staining of inflammatory-related markers was performed at 1 week and 4 weeks to evaluate the inflammatory response of the grafts with different pore sizes at the short- and long-term. The results showed CD68 (pan-macrophage marker), CCR7 (M1 phenotype marker) and CD163 (M2 phenotype marker) positive cells were all present in the grafts at 1 week and 4 weeks, but the macrophage polarization was different in grafts with different pore sizes at various time points after implantation (Fig. 4 A). The percentage of CD163 positive cells was significantly higher than the percentage of CCR7 positive cells in all grafts at 1 week and 4 weeks, and the percentage of CD163 positive cells in grafts with medium and large pore sizes was significantly higher than the grafts with small pore size at both 1 week and 4 weeks (Fig. 4 B and C). The ratio of CD163 to CCR7 macrophages present in the remodeling grafts with medium and large pore sizes was significantly higher than the grafts with small pore size at 1 week and 4 weeks (Fig. 4 D). These results indicated that the grafts with medium and large pore sizes possessed more constructive tissue remodeling outcomes, and are consistent with the findings of previous studies that have also found larger pores induce a higher ratio of M2 to M1 macrophages in other materials [11,12,44]. All the results obtained from the rat carotid interposition model demonstrated that though the three different types of grafts had high patency rates and the potential for vascular remodeling, the grafts with medium and large pore sizes achieved higher patency rates and more constructive tissue remodeling outcomes than the grafts with small pores at 1 week and 4 weeks. It is interesting to note that the grafts with small pores, which had the lowest dynamic compliance during mechanical characterization, performed least favorably of the three groups when implanted in the carotid artery.

Mid-term graft patency was evaluated using an abdominal aortic

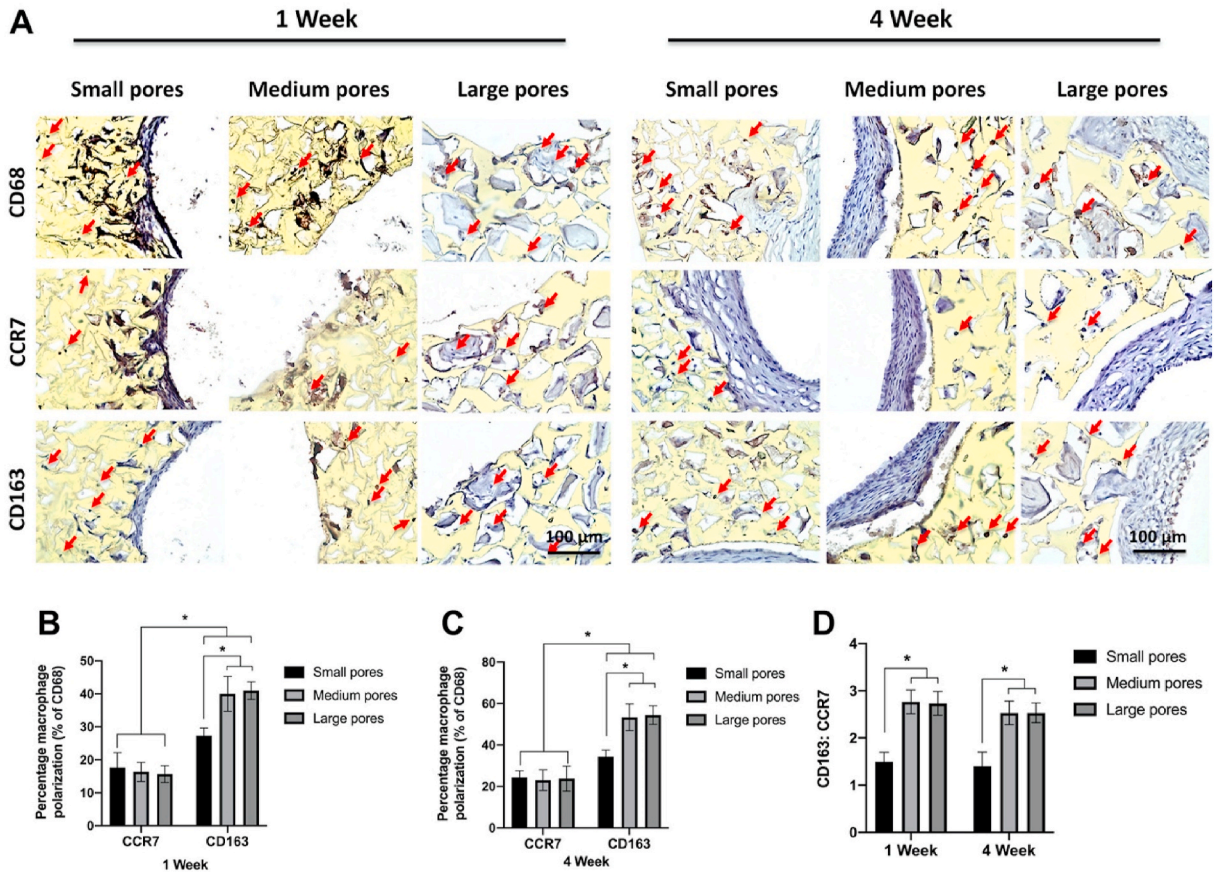

Fig. 4. (A) Inflammatory markers CD68, CCR7 and CD163 staining of the grafts at various time points after implantation. Yellow indicates the graft. Arrows indicate positive staining. Quantification of the percentage of macrophage polarization present in the remodeling grafts at (B) 1 week and (C) 4 weeks. (D) Quantification of the ratio of the percentage of CD163:CCR7 macrophages present in the remodeling grafts with different pore sizes at various time points after implantation. Each group at 1 week included 3 animals, and each group at 4 weeks included 6 animals. Data were expressed as mean ± standard deviation: *$p < 0.05$.

interposition model in rats using medium and large pore size grafts (n = 3 per group). Animals received heparin (100 U/kg) intraoperatively and once daily for two days postoperatively. Following implantation, grafts were monitored longitudinally using doppler ultrasound to assess blood velocity, distal aorta lumen diameter and blood flow rate through the graft (Fig. 5). Of the three rats that received large pore grafts, two died within the first 24 h and the remaining animal died on day four. Though unclear, the cause of failure for the large pore grafts may have been the leaking of blood from the sites of anastomosis under the increased pressure of the aortic environment following implantation. In contrast, all rats that received medium pore-size grafts survived and maintained graft patency for greater than 3 months. One rat in this group died of a ruptured peri-renal hematoma at 3.75 months; interestingly, the graft did not have any evidence of luminal thrombosis at the time of necropsy. The remaining two rats were sacrificed at 4 months.

Because the graft material is non-echogenic, ultrasound was not able to provide a direct measurement of blood velocity within the graft itself. Therefore, blood velocity and vessel diameter were measured in the aorta just distal to the graft. We found that the distal aorta lumen declined in diameter from 1.7 ± 0.15 mm at day 1–1.2 ± 0.07 mm at day 14 ($p = 0.02$). Following this, the average lumen diameter stabilized and reversed slightly to 1.4 ± 0.36 mm at 4 months, which was not significantly different from either the day 1 or day the 14 timepoints. A similar trend in mean flow rate was also observed, with an initial decline in flow followed by a recovery at 4 months. There was no significant change in mean blood velocity between the day 1 and 4-month timepoints (451 ± 154 vs. 733 ± 52.3 mm/s, $p = 0.18$). The observed reversal in the decline of the lumen diameter is consistent with a recent report on spontaneous resolution of stenosis in tissue engineered vascular grafts in an ovine interpositional model [45].

Histological staining of the grafts after 4 months showed neotissue development covering the entire lumen surface throughout the length of the grafts and joining with the native aortic tissue across the anastomoses (Fig. 6 A & B). Image analysis revealed the grafts maintained 81.1 ± 4.8% of the patent area compared with the bare polymer graft, some luminal loss occurring due to neovascular tissue development on the graft surface. The structure and composition of the neovessel tissue resembled a maturing arterial wall. Pentachrome staining showed regions of developing concentric layers and traces of elastin and collagen deposition. Further analysis by immunohistochemistry revealed positive staining for the endothelial cell marker CD31 on the luminal surface and the smooth muscle cell marker α-SMA within the wall of the developing neovessel tissue (Fig. 6C). The synthetic graft scaffold appears intact, with no visible signs of erosion, as expected from our DPY-PU materials, which demonstrate slow *in vitro* degradation, similar to the degradation profile of unmodified PCL [18]. Cellular infiltration was observed within the pores of the graft walls, with the deposition of intramural tissues resembling that of similarly slowly degrading synthetic vascular grafts [46–48]. In places, the cellular infiltration appeared inconsistent, with regions of little to no cellular ingrowth visible after 4 months, perhaps indicating excessive tortuosity or small windows connecting the larger pores, which is not uncommon in salt-leached porous scaffolds [5]. Strategies to include biomolecular cell signals or to create a more open route through the polymer wall, such as using a laser to punch direct channels, might encourage cellular repopulation within the vascular graft wall and enable integration of the SDVG lumen with surrounding microvascular beds. However, even without vascular infiltration into the graft wall, the robust neoarterial tissue observed and the

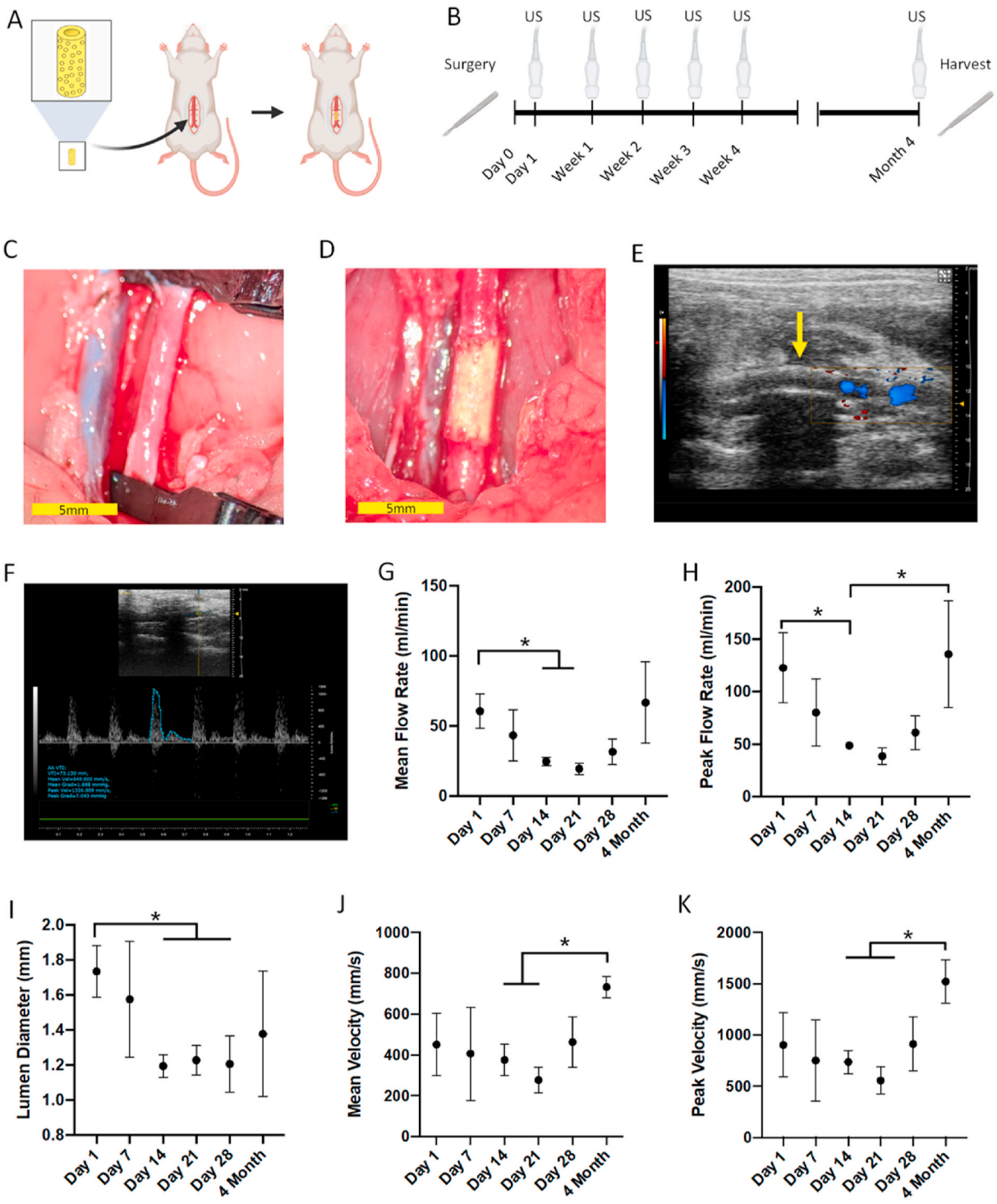

Fig. 5. (A) Aortic interposition model. (B) Ultrasound (US) analysis was performed at various time points postoperatively. (C) The rat abdominal aorta before and (D) after DPY-PU SDVG implantation. (E, F) Doppler ultrasound was used to measure the distal aorta flow velocity and diameter, confirming the grafts remained patent up to four months. The arrow points to the location of the vascular graft. US analysis yielded (G) mean flow rate, (H) peak flow rate, (I) lumen diameter, (J) mean blood flow velocity, and (K) peak blood flow velocity at various time points over the course of the four-month study. *Statistical significance ($p < 0.05$).

maintenance of blood flow for four months represent promising findings that support the potential of cell-free DPY-PU grafts to serve as vessel surrogates and supportive scaffolds for regenerating vascular tissue. These findings are especially promising, given that a recent meta-analysis of published SDVG studies found that the median SDVG implantation duration is only 56 days and 75% of synthetic grafts report occlusion [6]. Future work will need to evaluate the efficacy of DPY-PU grafts for longer time periods in rodents and in larger animal models more closely approximating humans. Based on our promising results, we also plan to perform short- and mid-term studies in both the rat carotid and aortic models in the future to gain a fuller understanding of tissue progression at both locations.

Excitingly, though the long term patency rate of our grafts is unknown, the maintenance of blood flow for four months may already demonstrate suitability for an alternative application of vascular grafts: providing blood flow to large engineered tissues and organs. Studies of

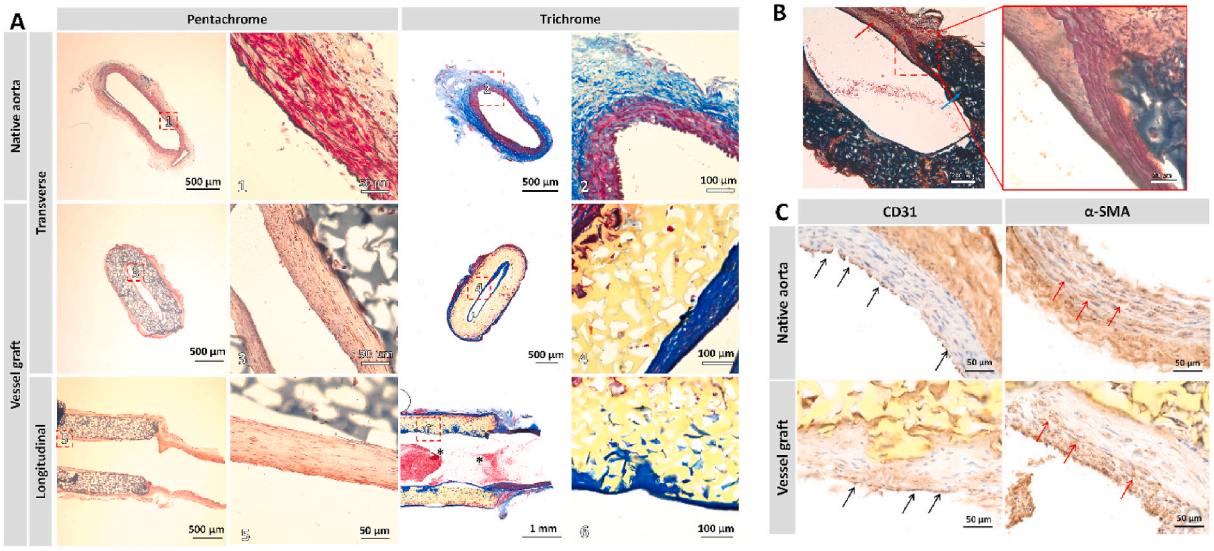

Fig. 6. Tissue remodeling of aortic graft. (A) Pentachrome and trichrome staining of the native aorta and DPY-PU SDVG showed neovessel tissue generation on the graft luminal surface that integrated with the native aortic wall across the anastomoses at the 4 month time point. Pentachrome: elastic fibers = black, nuclei = blue/black, collagen = yellow, mucin = bright blue, fibrin = bright red, muscle = red. DPY-PU stained black. Trichrome: cytoplasm and muscle fibers = red, collagen = blue. DPY-PU is yellow. *Residual blood left in lumen. (B) Pentachrome staining at 4 months showed continuous vessel wall tissue growth across the junction between the aorta (red arrow) and the vascular graft (blue arrow). (C) Immunohistochemical analysis of the neotissue development on the luminal surface of the DPY-PU vascular grafts at 4 months showed positive staining by DAB (stained brown, further indicated by arrows) for CD31 on the inner surface and α-SMA within the regenerating wall. Hematoxylin was used as a counterstain (purple).

transplanted vascularized free flaps indicate that reperfusion through the vascularized grafts following microsurgical anastomosis allows the grafts to survive and integrate with the surrounding tissue; and though the vascular anastomoses are at risk of occlusion, maintenance of blood flow within a vascularized graft for one month can typically provide sufficient time for graft survival via vessel ingrowth from the recipient wound bed into the graft [49]. Inclusion of a suturable synthetic blood vessel graft within large TE constructs to immediately establish blood flow might therefore similarly give life to implantable engineered tissues and organs.

3. Conclusion

Our DPY-PU grafts better match native blood vessel mechanics – combining both compliance and strength – compared with the current rigid clinical small diameter synthetic grafts and common biocompatible synthetic TE scaffold materials. When implanted in the carotid artery, the DPY-PU SDVGs remained patent at 1 week (the patency rate of all grafts with small, medium, and large pores = 100%) and demonstrated high patency rates at 4 weeks (small pore size group = 83%, medium pore size group = 100% and large pore size group = 100%). In an aortic interposition model, medium pore size grafts remained patent for four months and histological analysis showed regenerated vascular tissue with directionally oriented layers covering the luminal surface, demonstrating graft biointegration with the host arteries.

Tuning the pore size within the SDVGs impacted graft performance significantly. At 4 weeks post-implantation, DPY-PU grafts with small pores demonstrated reduced cellular infiltration into the vascular graft wall, smaller luminal diameter, and a higher proportion of proinflammatory macrophages compared with the grafts having medium and large pores. The grafts with large pores also demonstrated reduced calcification and increased numbers of SMCs with a contractile phenotype. While the large pore group demonstrated high levels of patency in the carotid context, when implanted in the abdominal aorta, three out of three grafts failed, demonstrating that necessary vascular graft properties vary based on implant site due to the heterogeneity of vascular environments throughout the body. By supporting robust vascular tissue regeneration and maintaining patency up to four months, the DPY-PU grafts show exciting promise for the next generation of vascular tissue engineering.

4. Methods

4.1. Graft fabrication

The polymer DPY-PU was prepared as previously reported [18]. Briefly, PCL (Mn 2000 Da; 0.9988 g, 0.5 mmol, 1 eq; Sigma-Aldrich, USA) was melted at 60 °C in a 20 mL flask equipped with stir bar, under N_2 atmosphere. N,N′-dimethylformamide (DMF; 1 mL; Acros Organics, Thermo Fisher Scientific, USA) was added followed by hexamethylene diisocyanate (HDI; 0.16 mL, 1.0 mmol, 2 eq; TCI, Japan). The solution was stirred for 2 h at 60 °C, at which point the vial was removed from the heat. Once cooled to room temperature, dipyridamole (DPY; 0.2520 g, 0.5 mmol, 1 eq; TCI) and an additional equivalent of HDI (0.08 mL, 0.5 mmol) was added. The solution was stored at 4 °C under N_2 until used.

The DPY-PU was processed into tubular grafts using a salt-leaching molding technique modified from Wu et al. [27] NaCl was first ground by mortar and pestle, then sieved through a series of nylon meshes (McMaster-Carr, USA) to obtain NaCl of various grain sizes (30–50 μm for the small pores, 50–80 μm for medium pores, 80–200 μm for large pores) which were then dried at 100 °C and stored in a vacuum desiccator.

The mold parts consist of glass tubing (ID = 1.6 mm; Wilmad-LabGlass, USA) cut into segments 5 cm long, two custom-made Teflon end-caps machined to fit tightly around the exterior of the glass tubing with a centered inner channel sized to fit a 1.5 mm diameter inner rod. The inner rod used was bend-resistant stainless steel coated with Teflon (McMaster-Carr). Dry salt was loaded into a segment of glass tubing with one end blocked by an endcap with the inner rod partially inserted to seal the hole. Once sufficiently filled with salt, the second endcap was put in place and the rod was gently pushed through the loose salt grains until it extruded through the second endcap. One endcap was then gently removed and the NaCl-loaded mold was placed in a humid fusion

chamber (95% humidity, 37 °C) for 45 min. The endcap was then gently replaced, the other one removed, and the mold placed back inside the fusion chamber for another 45 min. At this point the salt held its shape, keeping the inner rod in place and enabling both end caps to be removed. The molds were dried overnight at 100 °C, then placed in a vacuum desiccator until used.

To load the DPY-PU into the mold, the polymer solution was brought to room temperature, and then injected into the end of the mold (around the still inserted rod) using a segment of silicone tubing to connect the syringe to the glass tube. Once filled, the endcaps were placed back on and sealed with silicon grease, then the molds were placed in a 70 °C oven for 14 h to cure. Once fully solidified, the endcaps were removed and the molds were placed in a vacuum oven at 60 °C for another 14 h, after which the polymer was allowed to cool to room temperature and then the inner rods were removed. The glass tubing and polymer were placed in a DI water bath at room temperature for 14 h, after which the polymers tubes could be demolded.

To remove any residual NaCl, the polymer grafts were submerged in a DI H_2O bath for a further 48 h, with the water changed twice daily. The grafts were then snap frozen in liquid N_2 and lyophilized to dryness. Grafts were sterilized by autoclave (steam, 121 °C) prior to all characterization and implantation procedures.

4.2. Structural characterization

DPY-PU segments were cut by razor blade, sputter coated in Pd/Au (DeskII, Denton, USA), and imaged by scanning electron microscopy (SEM; Sigma FESEM, Zeiss, Germany). SEM images were used to measure graft dimensions and characterize the pore structure using ImageJ software. Micro-computed tomography (micro-CT; 40 kV, 200 μA, 396 ms; Skyscan, Bruker, USA) scans were carried out with an isotropic voxel size of 4 μm^3. The instrument software was used to measure graft porosity.

4.3. Mechanical characterization

To measure the effective elastic modulus, grafts were analyzed by unidimensional tensile testing on an Instron 5565 fitted with a 100 N load cell. Grafts were sliced longitudinally and unrolled to yield rectangular sheets, which were distended at a rate of 10 mm/min. To measure suture retention, tubular graft segments were pierced 2 mm from the end and a 9–0 nylon suture (Ningbo Medical Needle, China) was drawn through one wall to form a loop. The unsutured graft end and suture loop were then secured in the grips of an Instron 5565 mechanical tester and pulled at a rate of 10 mm/min until the suture broke completely free from the polymer wall. The maximum force measured was recorded as the suture retention force.

Due to their interconnected pore networks, the DPY-PU grafts demonstrate permeability to water; to measure compliance and burst pressure, specimens were first sealed by applying a layer of fibrin to plug the pores. To do this, DPY-PU tubes were mounted on an inner rod to fill the inner luminal space and were then submerged in a solution of fibrinogen (70 mg/mL; from bovine serum; Sigma-Aldrich) for 14 h at 4 °C. Grafts were then transferred to a thrombin solution (500 IU/mL; from bovine serum; Sigma-Aldrich) for 30 min.

Graft compliance was measured using a custom testing system as previously reported [50]. The fibrin-sealed DPY-PU tubular segments were preheated to 37 °C and connected to a custom pressurization system. Throughout the testing, grafts were submerged in a bath of phosphate buffered saline (PBS) maintained at 37 °C. Fluid pressurization was achieved using a flexible bellows connected to an Instron ElectroPuls E10000 and the pressure was recorded with a transducer (PX309-005G5V, Omega Engineering, USA). The graft outer diameter was monitored using a CCD camera (acA1600-20 gm, Basler, USA). Specimens were dynamically pressurized from 80 to 120 mmHg at 1 Hz for 50 cycles. The dynamic compliance (DC) was then calculated as the mean percent change in graft outer diameter for the last five loading cycles. DC (%/100 mmHg) = $[(D_2 - D_1)/D_1] * [1/(P_2 - P_1)] * 10^4$, where D_2 and D_1 are the graft outer diameters at the high ($P_2 = 120$ mmHg) and low ($P_1 = 80$ mmHg) pressures, respectively.

To measure burst pressures, the fibrin-coated SDVG were pressurized by syringe pump (NE-1010, New Era Pump Systems, USA) at a rate of 50 mL/min. Burst pressure was defined as the maximum pressure recorded prior to graft rupture.

4.4. Cytocompatibility

To confirm that porous DPY-PU is a suitable substrate for cellular attachment and proliferation, *in vitro* cell culture of HUVEC (passage 5; gift from Folkmann lab [51]) and hMSC (passage 7; Lonza, Switzerland) were carried out. Flat DPY-PU samples were cut from a prepared sheet of DPY-PU using a 5 mm biopsy punch and fixed to the bottom of 96 well plates using silicon grease. Cells were seeded at a density of 2.6 x 10^3 cells/cm^2. HUVEC were cultured in endothelial growth media (endothelial cell basal medium 2 + SupplementPack endothelial cell GM2; PromoCell, Germany) and hMSC were cultured in DMEM (Life Technologies, Thermo Fisher Scientific, USA) supplemented with fetal bovine serum (10%; Life Technologies) and penicillin-streptomycin-glutamine (1%; Life Technologies). Cell counts at day 1, 4, and 7 were measured by PicoGreen DS DNA assay (Invitrogen, Thermo Fisher Scientific, USA).

4.5. Animal care

All carotid animal experiments were approved by the Institutional Animal Care and Use Committee at the University of California, Davis. Male Sprague-Dawley rats (weight, 350–400 g; Charles River, USA) were used for these surgeries. All aortic animal experiments at were performed at the Hagey Laboratory for Pediatric Regenerative Medicine at Stanford University and were approved by the Stanford Administrative Panel on Laboratory Animal Care (APLAC #30462). Surgeries were performed on 6 Wistar rats (Charles River Laboratories) weighing 250–350 g (ages 10–14 weeks). Animal were kept at a 12 h dark/light cycle and had free access to food and water.

4.6. Carotid interposition surgery

As described in our previous work [38], the rats were anesthetized with 2.0% isoflurane and their body temperature was maintained at 37.5 °C using a heating pad. The left common carotid artery of each rat was dissected freely and clamped at the proximal and distal ends. After removing the common carotid artery, a pre-sterilized DPY-PU vascular graft trimmed to 5–6 mm was implanted by end-to-end anastomosis using a 10–0 needle and the circulation was restored. At 1 week and 4 weeks after graft implantation, the implantation site was reopened to determine the patency of the grafts. The patency of the graft was determined by examining the blood flow in the vessel at the distal end of the graft in the live animal under anesthesia. The graft was defined as patent if there was a restoration of blood flow in the distal vessel after squeezing and releasing the vessel with forceps. In detail, a set of fine forceps was used to hold the native blood vessel near the distal anastomotic site. The other set of forceps was used to squeeze the vessel gently from the hold site toward the head side of the animal for about 3–5 mm, causing the blood vessel to flatten. The forceps used to hold the native blood vessel near the distal anastomotic site were then released to determine whether blood flow could be restored to inflate the vessel. The animals were then euthanized, and the vascular grafts were explanted.

4.7. Histological and immunohistological analysis of the carotid grafts

Samples for histological examination were fixed with 10% formalin (ThermoFisher Scientific, USA), dehydrated by 30% sucrose solution

(ThermoFisher Scientific, USA), snap-frozen in optimal cutting temperature (OCT) compound and cross sectioned into 10 μm thickness using a cryostat. The standard H&E (ThermoFisher Scientific, USA), Trichrome (ThermoFisher Scientific, USA) and Modified Russell-Movat Pentachrome (Abcam, UK) staining were performed to analyze the cellularity, tissue remodeling and the patency of grafts according to the manufacturer protocols. Immunohistological staining for CD31, α-SMA, CD68, CCR7 and CD163 was performed using primary antibody (Abcam, UK) and secondary antibody (horseradish peroxidase-conjugated, Abcam, UK). Secondary antibody was detected by reaction with 3,3′-diaminobenzidine (DAB, Abcam, UK). Mayer's Hematoxylin (ThermoFisher Scientific, USA) was used as a counterstain. Images were captured using the Keyence digital microscope (USA). Quantification was performed using the Image J software.

4.8. Aortic interposition surgery

Aortic surgery was performed with a surgical microscope under 10x magnification (Leica M500 N OHS-1, Leica Microsystems, Germany) under inhalation anesthesia with isoflurane (4% and 2%) with 2 L/min oxygen. Animals received heparin (100 IU/kg, subcutaneous), buprenorphine (0.05 mg/kg, subcutaneous), enrofloxacin (5 mg/kg, subcutaneous), and normal saline (10 ml/kg, subcutaneous) following induction of anesthesia. An additional bolus of normal saline (10 ml/kg, subcutaneous) was administered at the conclusion of surgery, and again on postoperative day 1. At the end of the experiments, euthanasia was achieved by exsanguination from distal aortic transection during graft harvest as well as cardiac puncture under deep anesthesia.

Following induction of anesthesia, rats were laid supine and their abdomen shaved. A chemical depilating agent (Nair™, Church and Dwight, USA) was used to remove any remaining hair. The abdomen was prepped with betadine and draped sterilely. Surgery was performed using a sterile tips-only approach. A midline incision was made from the xiphoid to the symphysis pubis. The incision was carried down sharply through the linea alba, using bipolar electrocautery for hemostasis. Upon entry to the abdominal cavity the small and large intestines were gently transposed outside of the abdomen onto a saline moistened gauze, which was intermittently irrigated throughout the procedure. Gentle spreading of retroperitoneal fat was performed with cotton tipped applicators to expose the abdominal aorta and inferior vena cava (IVC). The aorta was further exposed and mobilized from the renal arteries down to the iliac bifurcation using microsurgical dissection technique. Posterior lumbar spinal arteries were carefully identified and coagulated with bipolar as needed to further mobilize the vessel. Microvascular clamps were placed on the aorta on the infrarenal segment, and the aorta was sharply transected. The vessel lumen was irrigated with heparinized saline (5000 IU/ml) and the vessel adventitia trimmed as needed for the anastomosis. Next, a pre-sterilized DPY-PU vascular graft trimmed to a length of 5 mm was introduced into the field. Microsurgical anastomosis was performed in an end-to-end manner with a series of interrupted 10–0 nylon sutures. The lumen was flushed with heparinized saline (5000 IU/ml) prior to tying down the final suture. The clamps were released, and patency of flow confirmed by observation of pulsatility and a double occlusion test. The field was irrigated with saline and the intestines returned to the abdominal cavity. The incision was then closed in layers with a simple running 4–0 vicryl for the abdominal wall and a running 3–0 prolene for the skin. The wound was dressed with Telfa™ (Covidien, Ireland) and Tegaderm™ (3M, USA) and the dressing was changed on postoperative day 1 and removed on postoperative day 5. The rats received subcutaneous heparin (100 U/kg) and normal saline (5 ml/kg) once daily for two days postoperatively.

To harvest the grafts four months following implantation, the rats were then placed under deep anesthesia and the grafts were exposed surgically and in sterile fashion as previously described. After exposing the graft, the distal aorta was transected sharply to confirm blood flow patency through the graft. The aorta proximal to the graft was then transected and the graft with adjacent aortic tissue harvested and prepared for histological evaluation.

4.9. Aortic ultrasound measurements

Early graft patency was assessed on postoperative day 1, 7, 14, 21, and 28 using ultrasound. Animals were anesthetized with inhalational anesthesia as previously described and placed supine on the imaging platform. The abdomen was clipped of any hair as needed prior to imaging. Imaging was performed using a Vevo 2100 high-resolution ultrasound (VisualSonics, Canada) with an MS-250 MHz transducer. Pulsed-Wave doppler mode was used to measure the velocity-time interval (VTI) of the aorta just distal to the interposition graft. Flow within the graft itself was unable to be measured ultrasonically due to the acoustic effects of the graft material, so the distal aorta was selected for flow measurement. The vessel lumen diameter at the same point where the VTI was measured using B-mode. Additional representative images were taken of the graft and aorta along its longitudinal axis using B-mode and color mode. Using the measured average flow velocity and vessel diameter, the flow rate was calculated using the following equation:

$$\text{Flow rate } (\text{ml}/\text{min}) = \frac{1}{4} * \pi * \text{vessel diameter } (\text{mm})^2 * \text{average blood velocity } (\text{mm}/\text{s})$$

4.10. Histological and immunohistochemical evaluation of the aortic grafts

The vascular grafts and adjacent aortic tissue were fixed in 4% paraformaldehyde overnight at 4 °C, followed by embedding in OCT compound and sectioning into 10 μm longitudinal and transverse sections on a cryotome. Modified Russell-Movat pentachrome (Abcam, UK) and trichrome (Sigma-Aldrich) staining were performed according to the manufacturer protocols. IHC staining for CD31 and α-SMA was performed using primary antibody (mouse anti-rat; Santa Cruz Biotechnology, USA) and secondary antibody (horseradish peroxidase-conjugated goat anti-mouse; Abcam). Secondary antibody was detected by reaction with 3,3′-diaminobenzidine (DAB, Thermo Fisher Scientific). Mayer's Hematoxylin (Sigma-Aldrich) was used as a counterstain.

4.11. Statistical analysis

Statistical analysis was performed using SPSS (IBM, USA). Values are presented as the means ± standard deviations, unless otherwise noted. Statistical significance of pre-operative graft characterization was determined by one-way ANOVA with Tukey's post-hoc test. Statistical significance between post-operative ultrasound measurements was calculated by Student t-test. *p*-values less than 0.05 were considered significant.

CRediT authorship contribution statement

Alexander Stahl: Conceptualization, Formal analysis, Investigation, Methodology, Project administration, Validation, Visualization, Writing – original draft, Writing – review & editing. **Dake Hao:** Conceptualization, Formal analysis, Investigation, Methodology, Validation, Visualization, Writing – original draft, Writing – review & editing. **Janos Barrera:** Methodology, Formal analysis, Investigation, Visualization, Writing – original draft. **Dominic Henn:** Methodology, Investigation. **Sien Lin:** Investigation. **Seyedsina Moeinzadeh:** Conceptualization. **Sungwoo Kim:** Investigation. **William Maloney:** Conceptualization. **Geoffrey Gurtner:** Conceptualization, Supervision. **Aijun Wang:** Conceptualization, Supervision, Funding acquisition. **Yunzhi Peter Yang:** Conceptualization, Supervision, Funding acquisition.

Declaration of competing interest

Conflicts of interest: none.

Acknowledgments

This research was partially funded through financial support from NIH grants R01AR057837, U01AR069395, R01AR072613, and R01AR074458 from NIAMS, and DoD grant W81XWH-20-1-0343, the Stanford Woods Institute for the Environment, and the Tad and Diane Taube Family Foundation.

Appendix B. Supplementary data

Supplementary data to this article can be found online at https://doi.org/10.1016/j.bioactmat.2022.04.004.

Appendix A. Supplementary Information

Supplementary data related to this article may be found online.

References

[1] D.N. Ghista, F. Kabinejadian, Coronary artery bypass grafting hemodynamics and anastomosis design: a biomedical engineering review, Biomed. Eng. Online 12 (2013) 129.
[2] P.M. Crapo, Y. Wang, Physiologic compliance in engineered small-diameter arterial constructs based on an elastomeric substrate, Biomaterials 31 (2010) 1626–1635.
[3] S. Pashneh-Tala, S. MacNeil, F. Claeyssens, The tissue-engineered vascular graft—past, present, and future, Tissue Eng. B Rev. 22 (2016) 68–100.
[4] S. Greenwald, C. Berry, Improving vascular grafts: the importance of mechanical and haemodynamic properties, J. Pathol. 190 (2000) 292–299.
[5] P. Zilla, D. Bezuidenhout, P. Human, Prosthetic vascular grafts: wrong models, wrong questions and no healing, Biomaterials 28 (2007) 5009–5027.
[6] I. Skovrind, E.B. Harvald, H. Juul Belling, et al., Concise review: patency of small-diameter tissue-engineered vascular grafts: a meta-analysis of preclinical trials, Stem cells transl. med. 8 (2019) 671–680.
[7] S. Mitragotri, J. Lahann, Physical approaches to biomaterial design, Nat. Mater. 8 (2009) 15–23.
[8] L. Zhen, S.A. Creason, F.I. Simonovsky, et al., Precision-porous polyurethane elastomers engineered for application in pro-healing vascular grafts: synthesis, fabrication and detailed biocompatibility assessment, Biomaterials 279 (2021), 121174.
[9] T.C. Boire, L.E. Himmel, F. Yu, et al., Effect of pore size and spacing on neovascularization of a biodegradble shape memory polymer perivascular wrap, J. Biomed. Mater. Res. 109 (2021) 272–288.
[10] M.A. Contreras, W.C. Quist, F.W. Logerfo, Effect of porosity on small-diameter vascular graft healing, Microsurgery: Off. J. Int. Microsurg. Soc. Europ. Feder. Soci. Microsurg. 20 (2000) 15–21.
[11] Y. Yin, X.-T. He, J. Wang, et al., Pore size-mediated macrophage M1-to-M2 transition influences new vessel formation within the compartment of a scaffold, Appl. Mater. Today 18 (2020), 100466.
[12] K. Garg, N.A. Pullen, C.A. Oskeritzian, et al., Macrophage functional polarization (M1/M2) in response to varying fiber and pore dimensions of electrospun scaffolds, Biomaterials 34 (2013) 4439–4451.
[13] E.M. Sussman, M.C. Halpin, J. Muster, et al., Porous implants modulate healing and induce shifts in local macrophage polarization in the foreign body reaction, Ann. Biomed. Eng. 42 (2014) 1508–1516.
[14] K. Ota, Y. Sasaki, Y. Nakagawa, et al., A completely new poly (ether-urethane) graft ideal for hemodialysis blood access, Am. Soc. Artif. Intern. Organs J. 33 (1987) 129–135.
[15] Z. Wang, Y. Cui, J. Wang, et al., The effect of thick fibers and large pores of electrospun poly (ε-caprolactone) vascular grafts on macrophage polarization and arterial regeneration, Biomaterials 35 (2014) 5700–5710.
[16] O. Oliviero, M. Ventre, P. Netti, Functional porous hydrogels to study angiogenesis under the effect of controlled release of vascular endothelial growth factor, Acta Biomater. 8 (2012) 3294–3301.
[17] S. Boersema, F. Lange, Bastiaansen-Jenniskens, The effect of biomaterials used for tissue regeneration purposes on polarization of macrophages, BioResearch Open Access (2016).
[18] A.M. Stahl, Y.P. Yang, Tunable elastomers with an antithrombotic component for cardiovascular applications, Adv. healthc. mater. 7 (2018), 1800222.
[19] M.C. Wake, C.W. Patrick Jr., A.G. Mikos, Pore morphology effects on the fibrovascular tissue growth in porous polymer substrates, Cell Transplant. 3 (1994) 339–343.
[20] T. Ma, Y. Li, S.T. Yang, et al., Tissue engineering human placenta trophoblast cells in 3-D fibrous matrix: spatial effects on cell proliferation and function, Biotechnol. Prog. 15 (1999) 715–724.
[21] T. Ma, Y. Li, S.T. Yang, et al., Effects of pore size in 3-D fibrous matrix on human trophoblast tissue development, Biotechnol. Bioeng. 70 (2000) 606–618.
[22] Y. Luo, G. Engelmayr, D.T. Auguste, et al., 3D Scaffolds. Principles of Tissue Engineering, Elsevier, 2014, pp. 475–494.
[23] E. Tsuruga, H. Takita, H. Itoh, et al., Pore size of porous hydroxyapatite as the cell-substratum controls BMP-induced osteogenesis, J. Biochem. 121 (1997) 317–324.
[24] E.H. Phillips, A.A. Yrineo, H.D. Schroeder, et al., Morphological and biomechanical differences in the elastase and AngII apoE−/− rodent models of abdominal aortic aneurysms, BioMed. res. int. 2015 (2015).
[25] J. Zhao, J. Day, Z.F. Yuan, et al., Regional arterial stress-strain distributions referenced to the zero-stress state in the rat, Am. J. Physiol. Heart Circ. Physiol. 282 (2002) H622–H629.
[26] N. Uchida, H. Emoto, H. Kambic, et al., Compliance effect on patency of small diameter vascular grafts, ASAIO transact. 35 (1989) 556–558.
[27] W. Wu, R.A. Allen, Y. Wang, Fast-degrading elastomer enables rapid remodeling of a cell-free synthetic graft into a neoartery, Nat. Med. 18 (2012) 1148.
[28] K.-W. Lee, P.S. Gade, L. Dong, et al., A biodegradable synthetic graft for small arteries matches the performance of autologous vein in rat carotid arteries, Biomaterials 181 (2018) 67–80.
[29] A. Nieponice, L. Soletti, J. Guan, et al., In vivo assessment of a tissue-engineered vascular graft combining a biodegradable elastomeric scaffold and muscle-derived stem cells in a rat model, Tissue Eng. 16 (2010) 1215–1223.
[30] C.E. Stowell, Y. Wang, Quickening: Translational design of resorbable synthetic vascular grafts, Biomaterials 173 (2018) 71–86.
[31] N. Tai, H. Salacinski, A. Edwards, et al., Compliance properties of conduits used in vascular reconstruction, Br. J. Surg. 87 (2000) 1516–1524.
[32] N.R. Tai, A. Giudiceandrea, H.J. Salacinski, et al., In vivo femoropopliteal arterial wall compliance in subjects with and without lower limb vascular disease, J. Vasc. Surg. 30 (1999) 936–945.
[33] A. Tajaddini, D.L. Kilpatrick, P. Schoenhagen, et al., Impact of age and hyperglycemia on the mechanical behavior of intact human coronary arteries: an ex vivo intravascular ultrasound study, Am. J. Physiol. Heart Circ. Physiol. 288 (2005) H250–H255.
[34] L. Soletti, A. Nieponice, Y. Hong, et al., In vivo performance of a phospholipid-coated bioerodable elastomeric graft for small-diameter vascular applications, J. Biomed. Mater. Res. 96 (2011) 436–448.
[35] Y. Luo, D. Owens, G. Mulder, et al., Blood Pressure Characterization of Hypertensive and Control Rats for Cardiovascular Studies, AHA, Atlanta: Charles River, 2008.
[36] D.E. Anderson, J.J. Glynn, H.K. Song, et al., Engineering an endothelialized vascular graft: a rational approach to study design in a non-human primate model, PLoS One 9 (2014), e115163.
[37] A.M. Seifalian, A. Tiwari, G. Hamilton, et al., Improving the clinical patency of prosthetic vascular and coronary bypass grafts: the role of seeding and tissue engineering, Artif. Organs 26 (2002) 307–320.
[38] D. Hao, Y. Fan, W. Xiao, et al., Rapid endothelialization of small diameter vascular grafts by a bioactive integrin-binding ligand specifically targeting endothelial progenitor cells and endothelial cells, Acta Biomater. (2020).
[39] W. Gu, X. Hong, C. Potter, et al., Mesenchymal stem cells and vascular regeneration, Microcirculation 24 (2017), e12324.
[40] S. Hughes, T. Chan-Ling, Roles of endothelial cell migration and apoptosis in vascular remodeling during development of the central nervous system, Microcirculation 7 (2000) 317–333.
[41] E. Planas-Rigol, N. Terrades-Garcia, M. Corbera-Bellalta, et al., Endothelin-1 promotes vascular smooth muscle cell migration across the artery wall: a mechanism contributing to vascular remodelling and intimal hyperplasia in giant-cell arteritis, Annals of the rheumatic diseases 76 (2017) 1624–1634.
[42] B.N. Brown, R. Londono, S. Tottey, et al., Macrophage phenotype as a predictor of constructive remodeling following the implantation of biologically derived surgical mesh materials, Acta Biomater. 8 (2012) 978–987.
[43] B.N. Brown, J.E. Valentin, A.M. Stewart-Akers, et al., Macrophage phenotype and remodeling outcomes in response to biologic scaffolds with and without a cellular component, Biomaterials 30 (2009) 1482–1491.
[44] R. Liang, D. Fang, W. Lin, et al., Macrophage polarization in response to varying pore sizes of 3D polyurethane scaffolds, J. Biomed. Nanotechnol. 14 (2018) 1744–1760.

[45] J.D. Drews, V.K. Pepper, C.A. Best, et al., Spontaneous reversal of stenosis in tissue-engineered vascular grafts, Sci. Transl. Med. 12 (2020).
[46] T. Sugiura, S. Tara, H. Nakayama, et al., Novel bioresorbable vascular graft with sponge-type scaffold as a small-diameter arterial graft, Ann. Thorac. Surg. 102 (2016) 720–727.
[47] Y. Pan, X. Zhou, Y. Wei, et al., Small-diameter hybrid vascular grafts composed of polycaprolactone and polydioxanone fibers, Sci. Rep. 7 (2017) 1–11.
[48] F. Kuwabara, Y. Narita, A. Yamawaki-Ogata, et al., Long-term results of tissue-engineered small-caliber vascular grafts in a rat carotid arterial replacement model, J. Artif. Organs 15 (2012) 399–405.
[49] A.P. Yoon, N.F. Jones, Critical time for neovascularization/angiogenesis to allow free flap survival after delayed postoperative anastomotic compromise without surgical intervention: a review of the literature, Microsurgery 36 (2016) 604–612.
[50] Á.E. Mercado-Pagán, A.M. Stahl, M.L. Ramseier, et al., Synthesis and characterization of polycaprolactone urethane hollow fiber membranes as small diameter vascular grafts, Mater. Sci. Eng. C 64 (2016) 61–73.
[51] D.A. Freedman, J. Folkman, Maintenance of G1 checkpoint controls in telomerase-immortalized endothelial cells, Cell Cycle 3 (2004) 809–814.